

Successive-Cancellation Decoding of Reed-Muller Codes with Fast Hadamard Transform

Nghia Doan, Seyyed Ali Hashemi, and Warren J. Gross

Abstract—In this paper we propose efficient decoding techniques to significantly improve the error-correction performance of fast successive-cancellation (FSC) and FSC list (FSCL) decoding algorithms for short low-order Reed-Muller (RM) codes. In particular, we first integrate Fast Hadamard Transform (FHT) into FSC (FHT-FSC) and FSCL (FHT-FSCL) decoding algorithms to optimally decode the first-order RM subcodes. We then utilize the rich permutation group of RM codes by independently running the FHT-FSC and the FHT-FSCL decoders on a list of random bit-index permutations of the codes. The simulation results show that the error-correction performance of the FHT-FSC decoders on a list of L random code permutations outperforms that of the FSCL decoder with list size L , while requiring lower memory requirement and computational complexity for various configurations of the RM codes. In addition, when compared with the state-of-the-art recursive projection-aggregation (RPA) decoding, the permuted FHT-FSCL decoder can obtain a similar error probability for the RM codes of lengths 128, 256, and 512 at various code rates, while requiring several orders of magnitude lower computational complexity.

Index Terms—Reed-Muller codes, polar codes, 5G, successive cancellation decoding, permutations, fast Hadamard transform.

I. INTRODUCTION

Reed-Muller (RM) codes are a class of linear error-correction codes introduced by Muller [1] and Reed [2]. Under the factor-graph representation, RM codes are similar to polar codes [3] which are used in the enhanced Mobile Broadband (eMBB) scenario of the fifth generation (5G) cellular communication standard. The main difference between RM and polar codes is that RM codes are constructed to maximize the minimum distance of all the codewords [1], [2], while polar codes are constructed to minimize the error probability under successive-cancellation (SC) decoding [4], [5] or SC-list (SCL) decoding [6], [7]. Therefore, under maximum likelihood (ML) decoding, RM codes achieve a better error-correction performance than polar codes. However, ML decoding is generally impractical due to its high computational complexity.

RM codes can be decoded using a wide range of practical decoding algorithms as introduced in [8]–[11]. Recently, a recursive projection-aggregation (RPA) decoding algorithm [12] has been proposed that outperforms the error-correction performance of the decoders in [8]–[11]. RPA decoding relies on the code projections to recursively reduce the code order, where the Fast Hadamard Transform (FHT) algorithm is used to optimally decode the first-order RM codes [13]. To obtain the estimated codeword, RPA decoding aggregates the decoding outputs of various lower-order code projections based on a majority voting technique. It was shown in [12] that RPA decoding can obtain near ML decoding performance

for short and low-order RM codes, which also outperforms the error probability of the polar-cyclic redundancy check (CRC) concatenated codes under SCL algorithm at various code lengths and code rates. However, the main problems associated with RPA decoding are the high computational complexity, which significantly increases with the increase of the code rate, and the recursive nature of the algorithm, which hinders an efficient hardware implementation of the RPA decoder [14].

By sharing the same factor-graph representation with polar codes, RM codes can be decoded using the fast and low complexity decoding algorithms of polar codes, namely fast SC (FSC) [15] and fast SCL (FSCL) [16] decoding algorithms. However, the error probability of FSC and FSCL decoding with a small list size is inferior to that of RPA decoding, rendering the FSC-based algorithms to be unsuitable for applications with stringent frame error rate (FER) requirements. Although the FER of the FSCL decoders can be improved by increasing the list size, to obtain a FER performance close to that of RPA decoding, the list size required by FSCL decoding is impractical for RM codes of lengths greater than 128 [17]. To improve the error probability of RM codes under SC-based decoding, the received channel output can be decoded using the permuted factor-graph representations of the code [18]–[20]. This class of decoding algorithms requires various realizations of the decoders in hardware due to different permuted factor-graph representations. To address this problem, a one-to-one mapping between the permuted factor-graph representation and the permuted bit-index representation of the original factor-graph is introduced in [11], [21], which allows the use of a single architecture of the decoder in hardware. In [22], instead of performing the decoding on a list of factor-graph permutations, the authors provided a decoding algorithm that carefully selects a good factor-graph permutation on the fly, significantly improving the FER of SCL decoding with small list size. However, the FER of the decoder proposed in [22] is also inferior to that of RPA decoding.

In this paper, we focus on improving the error-correction performance of the low-complexity FSC and FSCL decoding algorithms with a small to moderate list size for RM codes. In particular, our proposed techniques are summarized as follows.

- 1) We first integrate FHT into FSC and FSCL decoding to optimally decode the first-order RM subcodes. We refer to this algorithm as FHT-FSC and FHT-FSCL decoding, respectively. We show that FHT-FSC and FHT-FSCL algorithms significantly improve the error-correction performance of the FSC and FSCL algorithms with a small list size for various code configurations.

2) To further improve the error-correction performance of FHT-FSC and FHT-FSCL decoding, we run the FHT-FSC and FHT-FSCL decoders on a list of random bit-index permutations of the codes. We show that the error-correction performance of FHT-FSC decoders on a list of L random permutations outperforms that of the state-of-the-art FSCL decoder with list size L , while requiring lower memory requirement and computational complexity under various configurations of RM codes. Furthermore, when compared with the RPA algorithm, the permuted FHT-FSCL decoder obtains a comparable error probability for the RM codes of lengths 128, 256, and 512 at various code rates, while requiring a computational complexity that is several orders of magnitude lower than that of RPA decoding.

The remainder of this paper is organized as follows. Section II introduces background on RM codes and their decoding algorithms. Section III provides the details of the proposed decoding techniques, followed by the experimental results presented in Section IV. Finally, concluding remarks are drawn in Section V.

II. PRELIMINARIES

A. Reed-Muller Codes

A RM code is specified by a pair of integers r and m , $0 \leq r \leq m$, and is denoted as $\mathcal{RM}(r, m)$, where r is the order of the code. $\mathcal{RM}(r, m)$ has a code length $N = 2^m$ with $K = \sum_{i=0}^r \binom{m}{i}$ information bits, and a minimum distance $d = 2^{m-r}$. Note that $\mathcal{RM}(m, m)$ is a rate-1 code that contains all the 2^N binary codewords of length N , and $\mathcal{RM}(-1, m)$ is a rate-0 code that contains the all-zero codeword of size N . A RM code can be constructed by applying a linear transformation to the binary message word $\mathbf{u} = \{u_0, u_1, \dots, u_{N-1}\}$ as $\mathbf{x} = \mathbf{u}\mathbf{G}^{\otimes m}$ where $\mathbf{x} = \{x_0, x_1, \dots, x_{N-1}\}$ is the codeword and $\mathbf{G}^{\otimes m}$ is the m -th Kronecker power of the matrix $\mathbf{G} = \begin{bmatrix} 1 & 0 \\ 1 & 1 \end{bmatrix}$ [23]. The element u_i of \mathbf{u} is fixed to 0 if the weight of the i -th row of $\mathbf{G}^{\otimes m}$, denoted as w_i , is smaller than d . Formally, $u_i = 0 \forall i \in \mathcal{F}$, where $\mathcal{F} = \{i | 0 \leq i < N, w_i < d\}$. In addition, we denote by \mathcal{I} the set of information bits, i.e., $\mathcal{I} = \{i | 0 \leq i < N, w_i \geq d\}$, and the sets \mathcal{I} and \mathcal{F} are known to both the encoder and the decoder.

In this paper, the codeword \mathbf{x} is modulated using binary phase-shift keying (BPSK) modulation, and additive white Gaussian noise (AWGN) channel model is considered. Therefore, the soft vector of the transmitted codeword received by the decoder is given as $\mathbf{y} = (\mathbf{1} - 2\mathbf{x}) + \mathbf{z}$, where $\mathbf{1}$ is an all-one vector of size N , and $\mathbf{z} \in \mathbb{R}^N$ is a Gaussian noise vector with variance σ^2 and zero mean. In the log-likelihood ratio (LLR) domain, the LLR vector of the transmitted codeword is given as $\boldsymbol{\alpha}_m = \ln \frac{Pr(\mathbf{x}=0|\mathbf{y})}{Pr(\mathbf{x}=1|\mathbf{y})} = \frac{2\mathbf{y}}{\sigma^2}$. Fig. 1(a) illustrates the encoding process of $\mathcal{RM}(1, 3)$ using the factor-graph representation of the code, where $N = 8$, $K = 4$, and $\mathcal{I} = \{3, 5, 6, 7\}$ [24].

B. Successive-Cancellation and Successive-Cancellation List Decoding

SC decoding is executed on the factor-graph representation of the code [3], [11]. To obtain the message word,

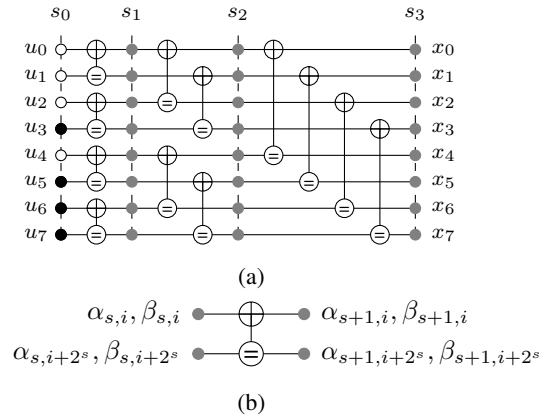


Fig. 1: (a) Factor-graph representation of $\mathcal{RM}(1, 3)$, and (b) a PE.

the soft LLR values and the hard bit estimations are propagated through all the processing elements (PEs), which are depicted in Fig. 1(b). Each PE performs the following computations: $\alpha_{s,i} = f(\alpha_{s+1,i}, \alpha_{s+1,i+2^s})$ and $\alpha_{s,i+2^s} = g(\alpha_{s+1,i}, \alpha_{s+1,i+2^s}, \beta_{s,i})$, where $\alpha_{s,i}$ and $\beta_{s,i}$ are the soft LLR value and the hard-bit estimation at the s -th stage and the i -th bit, respectively. The min-sum approximation formulations of f and g are $f(a, b) = \min(|a|, |b|) \text{sgn}(a) \text{sgn}(b)$, and $g(a, b, c) = b + (1 - 2c)a$. The soft LLR values at the m -th stage are initialized to α_m and the hard-bit estimation of an information bit at the 0-th stage is obtained as $\hat{u}_i = \beta_{0,i} = \frac{1 - \text{sgn}(\alpha_{0,i})}{2}$, $\forall i \in \mathcal{I}$. The hard-bit values of the PE are then computed as $\beta_{s+1,i} = \beta_{s,i} \oplus \beta_{s,i+2^s}$ and $\beta_{s+1,i+2^s} = \beta_{s,i+2^s}$.

Although SC decoding is a low-complexity decoding algorithm, its FER performance for short to moderate code lengths is mediocre. Therefore, SCL decoding was introduced to significantly improve the error-correction performance of SC decoding [11], [25], [26]. Under SCL decoding, the estimation of an information bit \hat{u}_i ($i \in \mathcal{I}$) is considered to be both 0 and 1, causing a path splitting and doubling the number of candidate codewords (decoding paths) after each split. To prevent the exponential growth of the number of decoding paths, a path metric is utilized to select the L most probable decoding paths after each information bit is decoded. In the LLR domain, the path metric is obtained as [26]

$$\text{PM}_l = \begin{cases} \text{PM}_l + |\alpha_{0,i_l}| & \text{if } \hat{u}_i \neq \frac{1 - \text{sgn}(\alpha_{0,i_l})}{2}, \\ \text{PM}_l & \text{otherwise,} \end{cases} \quad (1)$$

where α_{0,i_l} denotes the soft value of the i -th bit at stage 0 of the l -th path. Initially, $\text{PM}_l = 0, \forall l$. After each information bit is decoded, only L paths with the smallest path metric values are kept to continue the decoding. At the end of the decoding process, only the decoding path that has the smallest path metric is selected as the decoding output.

C. Fast Successive-Cancellation List Decoding

SCL decoding can also be illustrated using a binary tree representation [11], [15], [16], [27]. Fig. 2(a) shows a full binary tree representation of $\mathcal{RM}(1, 3)$, whose factor graph is depicted in Fig. 1(a). In [16], [28], the authors proposed

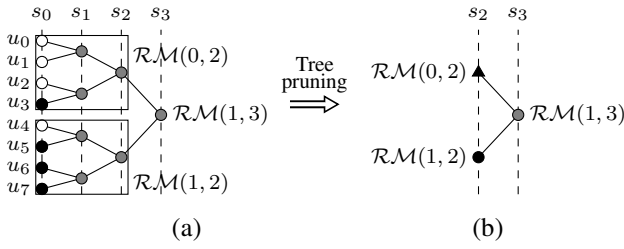


Fig. 2: (a) Full binary tree representation of $\mathcal{RM}(1,3)$ illustrated in Fig. 1(a), and (b) the pruned binary tree representation of the same RM code under FSCL decoding.

the FSCL decoding algorithms for various polar subcodes that can be directly applied to RM codes. For some special nodes, FSCL decoding preserves the error-correction performance of SCL decoding while completely removing the need to visit the descendant nodes. Therefore, the decoding latency of the FSCL algorithm is significantly reduced when compared with SCL decoding.

Consider a parent node ν located at the s -th stage ($s > 0$) of the binary tree, which is a $\mathcal{RM}(r_\nu, m_\nu)$. There are N_ν LLR values and N_ν hard decisions associated with this node, where $N_\nu = 2^{m_\nu} = 2^s$. Let α_{ν_l} and β_{ν_l} be the soft and hard values associated with a parent node ν of the l -th decoding path, respectively. α_{ν_l} and β_{ν_l} are given as

$$\begin{cases} \alpha_{\nu_l} = \{\alpha_{s, i_{\min_{\nu_l}}}, \dots, \alpha_{s, i_{\max_{\nu_l}}}\}, \\ \beta_{\nu_l} = \{\beta_{s, i_{\min_{\nu_l}}}, \dots, \beta_{s, i_{\max_{\nu_l}}}\}, \end{cases}$$

where $i_{\min_{\nu_l}}$ and $i_{\max_{\nu_l}}$ are the bit indices such that $0 \leq i_{\min_{\nu_l}} < i_{\max_{\nu_l}} \leq N - 1$ and $i_{\max_{\nu_l}} - i_{\min_{\nu_l}} = N_\nu - 1$. The hard-decision values of ν in the bipolar form are denoted as $\eta_{\nu_l} = \{\eta_{s, i_{\min_{\nu_l}}}, \dots, \eta_{s, i_{\max_{\nu_l}}}\}$, where $\eta_{s, i} = 1 - 2\beta_{s, i}$, $i_{\min_{\nu_l}} \leq i \leq i_{\max_{\nu_l}}$.

Note that under the binary-tree representation, the left-child of ν is $\mathcal{RM}(r_\nu - 1, m_\nu - 1)$ and the right-child of ν is $\mathcal{RM}(r_\nu, m_\nu - 1)$. If ν is neither a rate-0 nor a rate-1 code, the minimum and maximum order of ν is 0 and $m_\nu - 1$, respectively. Therefore, when applied to RM codes, the FSCL decoding algorithm of [16] only decodes $\mathcal{RM}(0, m_\nu)$, i.e., repetition (REP), and $\mathcal{RM}(m_\nu - 1, m_\nu)$, i.e., single parity check (SPC), codes. Let τ be the minimum number of path splittings that allows FSCL decoding to preserve the error-correction performance of the conventional SCL decoding algorithm. Also, let the elements of α_ν corresponding to the SPC nodes be sorted in the following order: $|\alpha_{s, i_{\min_{\nu_l}}}| \leq |\alpha_{s, i_{\min_{\nu_l}} + 1}| \leq \dots \leq |\alpha_{s, i_{\max_{\nu_l}}}|$. The decoding operations of the considered special nodes under FSCL decoding are summarized as follows.

1) $\mathcal{RM}(0, m_\nu)$ (REP): All the leaf nodes of a REP node are frozen bits, except for $\beta_{0, i_{\max_{\nu_l}}}$. The path metric of the l -th decoding path is calculated as [11], [16], [28]

$$\text{PM}_l = \text{PM}_l + \sum_{i=i_{\min_{\nu_l}}}^{i_{\max_{\nu_l}}} \frac{|\alpha_{s, i}| - \eta_{s, i_{\max_{\nu_l}}} \alpha_{s, i}}{2}, \quad (2)$$

where $\eta_{s, i_{\max_{\nu_l}}}$ denotes the bit estimate of the information bit of the REP node.

2) $\mathcal{RM}(m_\nu - 1, m_\nu)$ (SPC): All the leaf nodes of a SPC node are information bits, except for $\beta_{0, i_{\min_{\nu_l}}}$. The parity check sum of the l -th path is first obtained as [16], [28]

$$p_l = \bigoplus_{i=i_{\min_{\nu_l}}}^{i_{\max_{\nu_l}}} \frac{1 - \text{sgn}(\alpha_{s, i})}{2}. \quad (3)$$

The path metric is then updated as [16], [28]

$$\text{PM}_l = \begin{cases} \text{PM}_l + |\alpha_{s, i_{\min_{\nu_l}}}| & \text{if } p = 1, \\ \text{PM}_l & \text{otherwise.} \end{cases} \quad (4)$$

The decoding continues with τ path splittings, where $\tau = \min(L, N_\nu)$. In each new path splitting, the path metric is updated as [16], [28]

$$\text{PM}_l = \begin{cases} \text{PM}_l + |\alpha_{s, i}| + (1 - 2p_{s, i-1}) |\alpha_{s, i_{\min_{\nu_l}}}| & \text{if } \eta_{s, i} \neq \text{sgn}(\alpha_{s, i}), \\ \text{PM}_l & \text{otherwise,} \end{cases} \quad (5)$$

where $i_{\min_{\nu_l}} < i \leq i_{\min_{\nu_l}} + \tau$. The parity check sum is then updated after each path splitting as [28]

$$p_l = \begin{cases} 1 \oplus p_l & \text{if } \eta_{s, i_l} \neq \text{sgn}(\alpha_{s, i_l}), \\ p_l & \text{otherwise.} \end{cases} \quad (6)$$

When all the bits are estimated, the hard decision of the least reliable bit is updated to maintain the parity check condition of the SPC node, which is given as [16], [28]

$$\beta_{s, i_{\min_{\nu_l}}} = \bigoplus_{i=i_{\min_{\nu_l}}+1}^{i_{\max_{\nu_l}}} \beta_{s, i}. \quad (7)$$

Fig. 2(b) shows an example of the pruned binary tree representation of $\mathcal{RM}(1,3)$ depicted in Fig. 2(a), where FSCL decoding operations are applied to the REP and SPC nodes.

The memory requirements of FSC and FSCL decoding algorithms are given as [15], [26], [29]

$$\mathcal{M}_{\text{FSC}} = \underbrace{(2N - 1)Q}_{\alpha \text{ memory}} + \underbrace{N}_{\beta \text{ memory}}, \quad (8)$$

and

$$\begin{aligned} \mathcal{M}_{\text{FSCL}} &= \underbrace{(N + (N - 1)L)Q}_{\alpha \text{ memory}} + \underbrace{LQ}_{\text{PM memory}} + \underbrace{2NL}_{\beta \text{ memory}} \\ &= N(L + 1)Q + 2NL, \end{aligned} \quad (9)$$

where Q is the number of bits that are used to quantize the LLR and path metric values. In addition, we quantify the computational complexity of the FSC and FSCL decoders by counting the number of floating-point additions and comparisons required by the LLR sorting of the SPC nodes and the PM sorting of each path split.

D. Recursive Projection Aggregation Decoding

RPA decoding is an algorithm that can achieve near-ML decoding performance for low-order RM codes of short to moderate code lengths [12]. The RPA decoding algorithm performs iterative decoding operations on a set \mathbb{B} that contains

Algorithm 1: The RPA(\cdot) Decoding Algorithm [12]

Input : r, m, \mathbf{y}
Output: $\hat{\mathbf{x}}$

```

1 if  $r = 1$  then
2    $\hat{\mathbf{x}} \leftarrow$  Decode  $\mathbf{y}$  using FHT [13]
3 else
4   for  $i \leftarrow 0$  to  $\lceil \frac{m}{2} \rceil - 1$  do
5      $\mathbf{y}_{\text{agg}} \leftarrow \mathbf{0}$ 
6     for  $j \leftarrow 0$  to  $2^m - 2$  do
7       /* Projection */
8        $\mathbf{y}_{\mathbb{B}_j} \leftarrow \mathbf{0}$ 
9       for  $k \leftarrow 0$  to  $2^{m-1} - 1$  do
10         $\mathbf{y}_{\mathbb{B}_j}[k] \leftarrow$ 
11          Project( $\mathbf{y}[\mathbb{B}_{j,k,0}], \mathbf{y}[\mathbb{B}_{j,k,1}]$ )
12        /* Recursively decode  $\mathbf{y}_{\mathbb{B}_j}$  */
13         $\hat{\mathbf{x}}_{\mathbb{B}_j} \leftarrow$  RPA( $r-1, m-1, \mathbf{y}_{\mathbb{B}_j}$ )
14        /* Aggregation */
15        for  $k \leftarrow 0$  to  $2^{m-1} - 1$  do
16           $\mathbf{y}_{\text{agg}}[\mathbb{B}_{j,k,0}] \leftarrow$ 
17             $\mathbf{y}_{\text{agg}}[\mathbb{B}_{j,k,0}] + (1 - 2\hat{\mathbf{x}}_{\mathbb{B}_j}[k])\mathbf{y}[\mathbb{B}_{j,k,1}]$ 
18           $\mathbf{y}_{\text{agg}}[\mathbb{B}_{j,k,1}] \leftarrow$ 
19             $\mathbf{y}_{\text{agg}}[\mathbb{B}_{j,k,1}] + (1 - 2\hat{\mathbf{x}}_{\mathbb{B}_j}[k])\mathbf{y}[\mathbb{B}_{j,k,0}]$ 
20        /* Update  $\mathbf{y}$  and check for termination */
21         $\mathbf{y}_{\text{agg}} \leftarrow \frac{\mathbf{y}_{\text{agg}}}{2^{m-1}}$ 
22        if  $|\mathbf{y}_{\text{agg}}[j] - \mathbf{y}[j]| \leq \Delta|\mathbf{y}[j]| \forall j,$ 
23           $0 \leq j < 2^m - 1$  or  $i = \lceil \frac{m}{2} \rceil - 1$  then
24             $\hat{\mathbf{x}} \leftarrow$  Obtain hard decisions from  $\mathbf{y}_{\text{agg}}$ 
25            return  $\hat{\mathbf{x}}$ 
26        else
27           $\mathbf{y} \leftarrow \mathbf{y}_{\text{agg}}$ 
28 return  $\hat{\mathbf{x}}$ 

```

$2^m - 1$ one-dimensional code projections of $\mathcal{RM}(r, m)$, where the projected first-order RM codes are optimally decoded using the FHT algorithm [13]. Algorithm 1 provides the details of the RPA decoder introduced in [12].

Given $\mathcal{RM}(r, m)$ with $r > 1$ and the channel LLR vector \mathbf{y} , the RPA algorithm performs a maximum number of $\lceil \frac{m}{2} \rceil$ iterations. At each iteration i ($0 \leq i < \lceil \frac{m}{2} \rceil$), the decoder projects the channel LLR vector \mathbf{y} into the LLR vector $\mathbf{y}_{\mathbb{B}_j}$ corresponding to a projected $\mathcal{RM}(r-1, m-1)$ code by using the j -th projection of \mathbb{B} [12]. In this paper, we encode the one-dimensional projection set \mathbb{B} as a matrix of the elements $\mathbb{B}_{j,k,z}$. Specifically, $\mathbb{B}_{j,k,z}$ is the z -th element of the k -th coset that belongs to the j -th projection of \mathbb{B} , where $0 \leq z < 2$, $0 \leq k \leq 2^{m-1}$, and $0 \leq j \leq 2^m - 1$. Fig. 3 shows an example of the projection set \mathbb{B} of a RM code of length 8.

In Algorithm 1, the projected LLR vector $\mathbf{y}_{\mathbb{B}_j}$ is first initialized as an all-zero vector of size 2^{m-1} . The k -th element of $\mathbf{y}_{\mathbb{B}_j}$ is then calculated using the `Projection(\cdot)` function (line 9, Algorithm 1), where `Projection(a, b)` computes $\ln(\exp(a+b)+1) - \ln(\exp(a)+\exp(b))$ [12]. The estimated hard decision values of $\mathbf{y}_{\mathbb{B}_j}$ are recursively calculated by

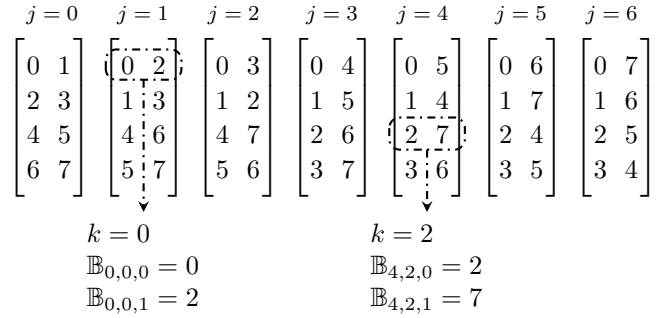


Fig. 3: Example of the one-dimensional projection set \mathbb{B} of a sized-8 RM code. An element of \mathbb{B} is indexed as $\mathbb{B}_{j,k,z}$ where $0 \leq j \leq 6$, $0 \leq k \leq 3$, and $0 \leq z \leq 1$.

running the RPA(\cdot) decoding function for $\mathbf{y}_{\mathbb{B}_j}$, followed by the aggregation step that updates the aggregated LLR vector \mathbf{y}_{agg} using the estimated values of $\hat{\mathbf{x}}_{\mathbb{B}_j}$ and the channel LLR vector \mathbf{y} (line 12 and 13, Algorithm 1) [12]. To reduce the decoding latency of RPA decoding, a convergence condition of \mathbf{y} and \mathbf{y}_{agg} is verified at each iteration (line 14, Algorithm 1), where Δ is a scaling factor used to ensure that \mathbf{y}_{agg} reaches a stable state [12]. If the termination condition is satisfied or the maximum number of iterations has been reached, the RPA decoder returns the estimated codeword by making the hard decisions from \mathbf{y}_{agg} , otherwise \mathbf{y} is updated as \mathbf{y}_{agg} and the decoder performs the next decoding iteration.

The memory requirement of RPA decoding under a sequential implementation is given as $\mathcal{M}_{\text{RPA}} = 4NQ + N$ [12]. In addition, we also count the number of floating-point additions/subtractions and floating-point comparisons to quantify the computational complexity of the RPA algorithm. In particular, the `Projection(a, b)` function requires 4 additions/subtractions as we consider the transcendental computations used in `Projection(a, b)` are implemented using a look-up-table (LUT) without degrading the FER performance. Each aggregation operation used in lines 12 and 13 of Algorithm 1 requires 1 addition. Furthermore, the FHT decoding algorithm, when applied to a $\mathcal{RM}(1, m)$, requires $m2^m$ additions and 2^m comparisons for the selection of the most probable codeword [13]. In this paper, we set $\Delta = 0.0625$ as opposed to 0.05 [12]. Therefore, a multiplication with Δ can be implemented by a low-cost shift operation. Consequently, the verification of the termination condition in line 15 of Algorithm 1 requires 2^{m+1} operations.

III. PROPOSED DECODING ALGORITHM

A. Improved FSCL Decoding with Fast Hadamard Transform

FHT decoding is a low-complexity ML decoding algorithm for first-order RM codes [13]. Note that a first-order RM code $\mathcal{RM}(1, s)$ located at the s -th stage of the binary tree can be decoded by first applying the FSCL decoding operations to the left-child REP node $\mathcal{RM}(0, s-1)$, followed by the FSCL decoding operations applied to the right-child SPC node $\mathcal{RM}(1, s-1)$ as specified in Section II-C. Given a small list size, the successive decoding order of FSCL results in a suboptimal estimated message word compared to that of FHT

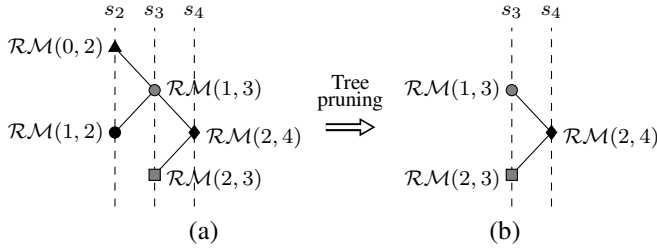


Fig. 4: The binary-tree representations of $\mathcal{RM}(2,4)$ under (a) FSCL and (b) FHT-FSCL decoding algorithms.

decoding. Therefore, in this section we propose a decoding algorithm that integrates FHT decoding into the conventional FSCL decoding algorithm to significantly improve the error-correction performance of the code given a small list size.

Fig. 4 illustrates an example of the proposed FHT-FSCL decoding algorithm for $\mathcal{RM}(2,4)$ under the binary-tree representation of the code. In Fig. 4(a), the conventional FSCL decoding algorithm is applied to $\mathcal{RM}(0,2)$, then to $\mathcal{RM}(1,2)$, and then to $\mathcal{RM}(2,3)$. On the other hand, the proposed FHT-FSCL decoding algorithm first performs FHT decoding on the first-order $\mathcal{RM}(1,3)$ subcode, followed by the conventional FSCL decoding operations of the SPC $\mathcal{RM}(2,3)$ node. Algorithm 2 provides the details of the proposed FHT-FSCL decoding algorithm with $L > 1$ when applied to a $\mathcal{RM}(1,s)$ sub code, also denoted as ν . We denote by L_{act} ($0 \leq L_{\text{act}} \leq L$) the number of decoding paths that are currently active before the $\mathcal{RM}(1,s)$ node is visited. Initially, $L_{\text{act}} = 1$. In addition, the inputs of Algorithm 2 contain the LLR values α_{ν_l} , and the path metric PM_l associated with the l -th decoding path, where $0 \leq l < L_{\text{act}}$.

In Algorithm 2, for each input path with index l , we perform FHT decoding using α_{ν_l} and generate the $\min(L, 2^s)$ most probable decoding paths and their associated path metrics originating from the l -th active decoding path. The details of the modified FHT decoding algorithm $\text{FHTD}(\cdot)$ is provided in Algorithm 3. In Algorithm 3, after the FHT operations are applied to α_{ν_l} , the indices of the largest absolute values of the transformed LLR values α_{ν_l} are obtained using a sorting algorithm (line 8, Algorithm 3). Note that we only need to construct a maximum of L best decoding paths generated from the current active path l under FHT decoding. Therefore, it is not necessary to sort all the elements of the transformed LLR values $|\alpha_{\nu_l}[i]|$ ($0 \leq i < N_\nu$) given a small list size L . Consequently, the complexity of the sorting algorithm used in line 9 of Algorithm 3 is $\min(L2^s, s2^s)$. Note that $L2^s$ is the number of comparisons required by a straightforward sorting algorithm that loops through the vector $|\alpha_{\nu_l}|$ L times to identify the indices of L maximum elements, while a maximum of $s2^s$ comparisons are required by the merge sort algorithm, which is more efficient for a large value of L . The sorting algorithm in line 9 of Algorithm 3 then outputs the sorted indices $\{i_0^*, \dots, i_{\min(L, 2^s)-1}^*\}$, where $|\alpha_{\nu_l}[i_0^*]| \geq \dots \geq |\alpha_{\nu_l}[i_{\min(L, 2^s)-1}^*]|$, and $\alpha_{\nu_l}[i]$ indicates the i -th element of α_{ν_l} . The indices $\{i_0^*, \dots, i_{\min(L, 2^s)-1}^*\}$ are then used to estimate the message words \hat{u}_ν associated with

Algorithm 2: FHT-FSCL Decoding of $\mathcal{RM}(1,s)$

Input : $\alpha_{\nu_l}, \text{PM}_l, L_{\text{act}}$ ($0 \leq l < L_{\text{act}}$)

Output: $\hat{x}_l, \text{PM}_l, L_{\text{act}}$ ($0 \leq l < L_{\text{act}}$)

```

/* Perform FHT decoding for each active
   decoding path */
1  $\mathcal{E} \leftarrow \emptyset$ 
2 for  $l \leftarrow 0$  to  $L_{\text{act}} - 1$  do
3    $\{\mathbf{Q}_0, \dots, \mathbf{Q}_{\min(L, 2^s)-1}\} \leftarrow \text{FHTD}(\alpha_{\nu_l}, \text{PM}_l, l)$ 
4    $\mathcal{E} \leftarrow \mathcal{E} \cup \{\mathbf{Q}_0, \dots, \mathbf{Q}_{\min(L, 2^s)-1}\}$ 
5    $\{\mathbf{Q}_0^*, \dots, \mathbf{Q}_{\min(L, 2^s L_{\text{act}})-1}^*\} \leftarrow \text{Sorting}(\mathcal{E})$ 
   /* Form the set of duplicated/discarded paths */
6    $\mathcal{L}_{\text{new}} \leftarrow \emptyset$ 
7   for  $i \leftarrow 0$  to  $L - 1$  do
8     if  $i \notin \{\mathbf{Q}_0^*\{l\}, \dots, \mathbf{Q}_{\min(L, 2^s L_{\text{act}})-1}^*\{l\}\}$  then
9        $\mathcal{L}_{\text{new}} \leftarrow \mathcal{L}_{\text{new}} \cup i$ 
   /* Path duplicating and killing operations */
10   $t \leftarrow 0, \mathcal{L}_{\text{org}} \leftarrow \emptyset$ 
11  for  $i \leftarrow 0$  to  $\min(L, 2^s L_{\text{act}}) - 1$  do
12     $l^* \leftarrow \mathbf{Q}_i^*\{l\}$ 
13    if  $l^* \notin \mathcal{L}_{\text{org}}$  then
14       $\mathcal{L}_{\text{org}} \leftarrow \mathcal{L}_{\text{org}} \cup l^*$ 
15       $\text{PM}_{l^*} \leftarrow \mathbf{Q}_i^*\{\text{PM}_\nu\}$ 
16       $\hat{x}_{l^*} \leftarrow \mathbf{Q}_i^*\{\hat{x}_\nu\}$ 
17    else
18       $\tilde{l} \leftarrow \mathcal{L}_{\text{new}}[t]$ 
19       $t \leftarrow t + 1$ 
20       $\text{PM}_{\tilde{l}} \leftarrow \mathbf{Q}_i^*\{\text{PM}_\nu\}$ 
21       $\hat{x}_{\tilde{l}} \leftarrow \mathbf{Q}_i^*\{\hat{x}_\nu\}$ 
22   $L_{\text{act}} \leftarrow \min(L, 2^s L_{\text{act}})$ 
23  return  $\hat{x}_l, \text{PM}_l, L_{\text{act}}$  ( $0 \leq l < L_{\text{act}}$ )

```

α_{ν_l} . $\text{dec2bin}(i)$ is a function that converts the decimal value of a bit index i to its binary expansion represented by s binary numbers. The path metric associated with each estimated message word is then calculated given \hat{x}_ν and α_{ν_l} as shown in line 18 of Algorithm 3 [16, Section II-D]. Algorithm 3 then outputs the most probable decoding paths under FHT decoding as a set of the data structure \mathbf{Q}_j , i.e., $\{\mathbf{Q}_0, \dots, \mathbf{Q}_{\min(L, 2^s)-1}\}$, where \mathbf{Q}_j consists of an estimated codeword \hat{x}_ν , its corresponding path metric PM_ν , and the index l of the active decoding path from which \hat{x}_ν is originated. Note that as a maximum of L best decoding paths are selected to continue the decoding after ν is visited, it is sufficient for Algorithm 3 to generate a maximum of L candidate paths associated with each LLR vector α_{ν_l} ($0 \leq l < L_{\text{act}}$).

In Algorithm 2, the outputs of the $\text{FHTD}(\cdot)$ function that is applied to all the current active paths are stored in a set \mathcal{E} . The sorting function applied to \mathcal{E} (line 5, Algorithm 2) generates a set of sorted data structures $\{\mathbf{Q}_0^*, \dots, \mathbf{Q}_{\min(L, 2^s L_{\text{act}})-1}^*\}$ such that $\mathbf{Q}_0^*\{\text{PM}_\nu\} \leq \dots \leq \mathbf{Q}_{\min(L, 2^s L_{\text{act}})-1}^*\{\text{PM}_\nu\}$, where $\mathbf{Q}_i^*\{\text{PM}_\nu\}$ indicates the path metric associated with the i -th data structure \mathbf{Q}_i^* . Also note that $l^* = \mathbf{Q}_i^*\{l\}$ and $\mathbf{Q}_i^*\{\hat{u}_\nu\}$ denote the index of the original decoding path l^* and the estimated message word \hat{u}_ν associated with $\alpha_{\nu_{l^*}}$, respectively.

Algorithm 3: Modified FHT Decoding of $\mathcal{RM}(1, s)$

```

Input :  $\alpha_\nu, \text{PM}_l, l$ 
Output:  $\{\mathbf{Q}_0, \dots, \mathbf{Q}_{\min(L, 2^s)-1}\}$ 
1 Function FHTD ( $\alpha_\nu, \text{PM}_l, l$ ):
   /* Fast Hadamard Transform of  $\alpha_{\nu_l}$  */
2   for  $t \leftarrow 0$  to  $s - 1$  do
3     for  $j \leftarrow 0$  to  $2^{t+1} - 1$  do
4       for  $i \leftarrow j2^{s-t}$  to  $j2^{s-t} + 2^{s-t-1} - 1$  do
5          $a \leftarrow \alpha_{\nu_l}[i + 2^{s-t-1}] - \alpha_{\nu_l}[i]$ 
6          $b \leftarrow \alpha_{\nu_l}[i + 2^{s-t-1}] + \alpha_{\nu_l}[i]$ 
7          $\alpha_{\nu_l}[i] \leftarrow a$ 
8          $\alpha_{\nu_l}[i + 2^{s-t-1}] \leftarrow b$ 
   /* Obtain up to  $L$  best decoding paths */
9    $\{i_0^*, \dots, i_{\min(L, 2^s)-1}^*\} \leftarrow \text{Sorting}(|\alpha_{\nu_l}|)$ 
10  for  $j \leftarrow 0$  to  $\min(L, 2^s) - 1$  do
   /* Form the estimated messageword  $\hat{\mathbf{u}}_\nu$  */
11   $m_s = \frac{1 - \text{sgn} \alpha_{\nu_l}[i_j^*]}{2}$ 
12   $\{m_{s-1}, \dots, m_0\} = \text{dec2bin}(2^s - 1 - i_j^*)$ 
13   $t \leftarrow 0$ 
14   $\hat{\mathbf{u}}_\nu \leftarrow \mathbf{0}$  // all-zero vector of size  $2^s$ 
15  for  $i \leftarrow 0$  to  $2^s - 1$  do
16    if  $i$  is an information bit then
17       $\hat{\mathbf{u}}_\nu[i] \leftarrow m_t$ 
18       $t \leftarrow t + 1$ 
19   $\hat{\mathbf{x}}_\nu \leftarrow \hat{\mathbf{u}}_\nu \mathbf{G}^{\otimes s}$ 
20   $\text{PM}_\nu \leftarrow \text{PM}_l + \sum_{i=0}^{2^s-1} (1 - 2\hat{\mathbf{x}}_\nu[i])\alpha_{\nu_l}[i]$ 
   /* Form the output data structure */
21   $\mathbf{Q}_j \leftarrow \{\hat{\mathbf{x}}_\nu, \text{PM}_\nu, l\}$ 
22  return  $\{\mathbf{Q}_0, \dots, \mathbf{Q}_{\min(L, 2^s)-1}\}$ 

```

In addition, we use the merge sort algorithm to output the sorted data structure \mathbf{Q}_i^* . Since the maximum size of \mathcal{E} is L^2 , the maximum number of floating-point comparisons required by the sorting operation in line 5 of Algorithm 2 is $2L^2 \log_2 L$.

The remainder of Algorithm 2 performs path killing and path duplicating operations, where we construct the sets of decoding path indices \mathcal{L}_{new} and \mathcal{L}_{org} . \mathcal{L}_{new} contains the indices of the paths that are currently inactive or discarded due to their high path metric values based on the path metric sorting carried out in line 5 of Algorithm 2. The path indices in \mathcal{L}_{new} are used to store the duplicated or new active decoding paths. \mathcal{L}_{org} is the set of the previous active decoding paths whose path metrics are among the L smallest ones stored in the data structure \mathbf{Q}_i^* . The number of current active decoding paths L_{act} is then updated at the end of Algorithm 2. Note that with $L = 1$, Algorithm 2 reverts to the conventional FHT decoding algorithm that only outputs the best candidate message word given by Algorithm 3. We refer to this special case of FHT-FSCL decoding as FHT-FSC decoding.

B. Improved FHT-FSCL Decoding with Code Permutations

Inspired by previous works [11], [19], [21], [30], we further improve the error-correction performance of the proposed

Algorithm 4: FHT-FSCL Decoding with Random Bit-Index Permutations

```

Input :  $M, \mathbf{y}$ 
Output:  $\hat{\mathbf{x}}$ 
   /* Construct a set  $\mathbb{P}$  of  $M$  different random
   bit-index permutations. */
1  $\mathbb{P} \leftarrow \emptyset$ 
2 while  $|\mathbb{P}| < M$  do
3    $\mathbf{I}_\pi \leftarrow \text{RandPer}()$ 
4   if  $\mathbf{I}_\pi \notin \mathbb{P}$  then
5      $\mathbb{P} \leftarrow \mathbb{P} \cup \mathbf{I}_\pi$ 
   /* Perform FHT-FSCL decoding using  $M$  random
   bit-index permutations */
6  $\hat{\mathbf{u}} \leftarrow \mathbf{0}, \mathbf{y}_\pi \leftarrow \mathbf{0}, \delta^* \leftarrow -\infty$ 
7 for all  $\mathbf{I}_\pi \in \mathbb{P}$  do
   /* Permute the channel LLR vector */
8   for  $j \leftarrow 0$  to  $N - 1$  do
9      $\mathbf{y}_\pi[j] \leftarrow \mathbf{y}[\mathbf{I}_\pi[j]]$ 
   /* Run FHT-FSCL decoding on  $\mathbf{y}_\pi$  */
10   $\hat{\mathbf{x}}_\pi \leftarrow \text{FHT-FSCL}(\mathbf{y}_\pi)$ 
   /* Calculate the reliability metric */
11   $\delta \leftarrow \sum_{j=0}^{N-1} (1 - 2\hat{\mathbf{x}}_\pi[j])\mathbf{y}_\pi[j]$ 
   /* Selection of the best message word */
12  if  $\delta^* < \delta$  then
13     $\delta^* \leftarrow \delta$ 
14    for  $j \leftarrow 0$  to  $N - 1$  do
15       $\hat{\mathbf{x}}[\mathbf{I}_\pi[j]] \leftarrow \hat{\mathbf{x}}_\pi[j]$ 
16 return  $\hat{\mathbf{x}}$ 

```

FHT-FSC and FHT-FSCL decoding algorithms by running the proposed decoders independently on a list of random bit-index permutations. Algorithm 4 outlines the improved FHT-FSCL decoding where the FHT-FSCL decoder is run on M different random bit-index permutations. In Algorithm 4, a set \mathbb{P} , which contains M different bit-index permutations, is constructed based on M different random factor-graph permutations of the code. The transformation from a factor-graph permutation to a bit-permutation is given in Algorithm 5. We denote by $\pi(\cdot)$ a permutation that randomly permutes the original indices of the PE layers, i.e., $\{0, \dots, n - 1\}$, and outputs the set S_π containing the permuted layer indices. Given S_π , the permuted bit-index set \mathbf{I}_π is constructed as shown in Algorithm 5 for all the bit indices $i, 0 \leq i < N - 1$. Note that the set \mathbb{P} is formed offline and is kept unchanged during the course of decoding. Fig. 5 illustrates examples of the permuted bit-index vectors \mathbf{I}_π generated by the `RandPer()` function when applied to $\mathcal{RM}(1, 3)$. The vectors \mathbf{I}_π are used to form the permuted bit-index of \mathbf{u} and \mathbf{x} , where the corresponding factor-graph permutations are $\{0, 2, 1\}$ and $\{1, 0, 2\}$ as shown in Fig. 5.

For each instance of the channel LLR vector \mathbf{y} , Algorithm 4 loops through each bit-index permutation $\mathbf{I}_\pi \in \mathbb{P}$ and permutes the indices of the channel LLR vector \mathbf{y} to generate \mathbf{y}_π . The proposed FHT-FSCL decoding algorithm is then used to decode \mathbf{y}_π and to estimate the permuted codeword $\hat{\mathbf{x}}_\pi$. When

Algorithm 5: Construct a random bit-index permutation [21]

```

1 Function RandPer():
  /* Obtain a factor-graph permutation */
2   $S_\pi \leftarrow \pi(\{0, \dots, n-1\})$ 
  /* Transform a factor-graph permutation to a
   bit-index permutation */
3   $I_\pi \leftarrow \emptyset$ 
4  for  $i \leftarrow 0$  to  $N-1$  do
5     $\{b_{n-1}^{(i)}, \dots, b_0^{(i)}\} \leftarrow \text{dec2bin}(i)$ 
6     $b_\pi^{(i)} \leftarrow \emptyset$ 
7    for  $j \leftarrow 0$  to  $n-1$  do
8       $b_\pi^{(i)} \leftarrow b_\pi^{(i)} \cup b_{S_\pi[j]}^{(i)}$ 
9     $I_\pi \leftarrow I_\pi \cup \text{bin2dec}(b_\pi^{(i)})$ 
10 return  $I_\pi$ 

```

$L = 1$, the FHT-FSCL decoder is replaced by the FHT-FSC decoder in line 10 of Algorithm 4. The likelihood of \hat{x}_π and \mathbf{y}_π , denoted as δ , is calculated in line 12 of Algorithm 4, where $x_\pi[j]$ and $\mathbf{y}_\pi[j]$ indicate the j -th element of \hat{x}_π and \mathbf{y}_π , respectively. The permuted codeword that has the maximum likelihood value δ^* is then selected as the final output after all the permutations are evaluated.

C. Computational Complexity and Memory Requirements

We summarize the computational complexities of all the decoding functions applied to a RM subcode of the proposed decoders in Table I and Table II. The computational complexities of the LLR and path metric calculations are represented as the number of floating-point additions, while the computational complexities of the sorting functions are calculated as the number of floating-point comparisons. To calculate the computational complexity of the FHT-FSC and FHT-FSCL decoders, the computational complexities of all the decoding functions are summed during the course of the decoding for a received channel LLR vector \mathbf{y} . In addition, the computational complexities of the permuted FHT-FSC and FHT-FSCL decoders that use M permutations are given as

$$\begin{cases} \mathcal{C}_{\text{p-FHT-FSC}} = M\mathcal{C}_{\text{FHT-FSC}} + M, \\ \mathcal{C}_{\text{p-FHT-FSCL}} = M\mathcal{C}_{\text{FHT-FSCL}} + M, \end{cases} \quad (10)$$

TABLE I: Computational complexities of different decoding functions required by the FHT-FSCL decoders with a list size $L > 1$. The decoding functions are applied to a RM sub-code $\mathcal{RM}(r, m)$ ($m \geq 0$) visited by the decoding algorithm.

Function	Computation		Sorting		Total
	LLR	Path Metric	LLR	Path Metric	
$f(\cdot)$	$L2^{m-1}$	-	-	-	$L2^{m-1}$
$g(\cdot)$	$L2^{m-1}$	-	-	-	$L2^{m-1}$
$\mathcal{RM}(0, m)$	$L(2^m - 1)$	L	-	$2L(1 + \log_2 L)$	$2L(2^{m-1} + \log_2 L + 1)$
$\mathcal{RM}(1, m)$	$Lm2^m$	$L2^{2m}$	$\min(Lm2^m, L^22^m)$	$2L^2 \log_2 L$	$Lm2^{m+1} + 2L^2(2^{m-1} + \log_2 L)$
$\mathcal{RM}(m-1, m)$	-	$L(1 + 2\tau)$	$\min(Lm2^m, L^22^m)$	$2\tau L(1 + \log_2 L)$	$L[m2^m + 2\tau(2 + \log_2 L) + 1]$

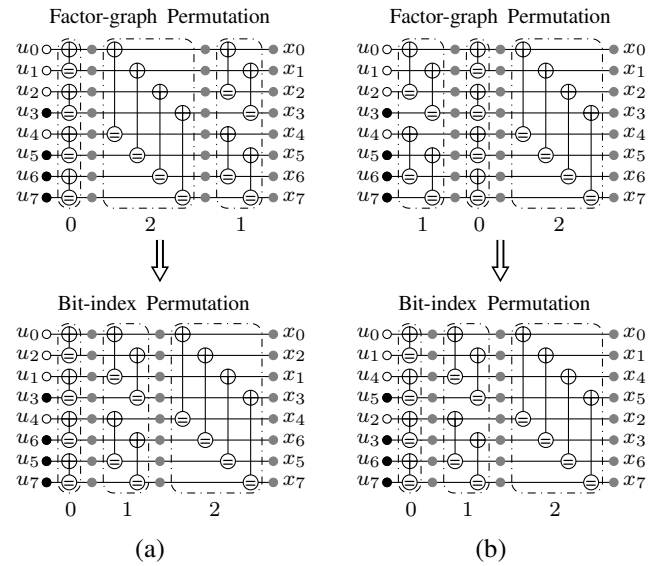


Fig. 5: The equivalent bit-index permutations of the factor-graph permutations (a) $\{0, 2, 1\}$ and (b) $\{1, 0, 2\}$, under the original factor-graph representation with the PE layers indexed as $\{0, 1, 2\}$.

where $\mathcal{C}_{\text{FHT-FSC}}$ and $\mathcal{C}_{\text{FHT-FSCL}}$ are the computational complexities of the FHT-FSC and FHT-FSCL decoders, respectively. Note that M floating-point comparisons are required for the permuted FHT-FSC and permuted FHT-FSCL decoders to select the codeword that has the maximum likelihood value.

The FHT used in Algorithm 3 only uses in-place computations that do not require extra memory for the LLR values [13]. Therefore, the memory requirements of the FHT-FSC and FHT-FSCL decoding algorithms are similar to those of FSC and FSCL decoding algorithms, respectively. In addition, under a sequential implementation the permuted FHT-FSC (p-FHT-FSC) and permuted FHT-FSCL (p-FHT-FSCL) decoding algorithms also consume the same amount of memory in comparison with the FHT-FSC and FHT-FSCL decoding algorithms, respectively. In this paper, we also consider a parallel implementation of the permuted FHT-FSC decoding algorithm, where L FHT-FSC decoders are run concurrently. Under this setting, the memory requirement of all the permuted FHT-FSC decoders is similar to that of FSCL decoding where we require LQ memory bits to store the likelihood values δ corresponding to L permutations. The memory requirements in terms of the number of bits of the proposed decoders are

TABLE II: Normalized computational complexities of different decoding functions under FSC and FHT-FSC decoders. The decoding functions are applied to a RM sub-code $\mathcal{RM}(r, m)$ ($m \geq 0$) visited by the decoding algorithm.

Function	LLR Computation	LLR Sorting	Total
$f(\cdot)$	2^{m-1}	-	2^{m-1}
$g(\cdot)$	2^{m-1}	-	2^{m-1}
$\mathcal{RM}(0, m)$	$2^m - 1$	-	$2^m - 1$
$\mathcal{RM}(1, m)$	$m2^m$	2^m	$2^m(m+1)$
$\mathcal{RM}(m-1, m)$	-	2^m	2^m

TABLE III: Summary of the memory requirements of the proposed decoders, where the parallel p-FHT-FSC decoding algorithm runs L FHT-FSC decoders concurrently.

Algorithm	Memory Requirement
FHT-FSC	$(2N-1)Q + N$
FHT-FSCL	$N(L+1)Q + 2NL$
p-FHT-FSC (sequential)	$2NQ + N$
p-FHT-FSC (parallel)	$N(L+1)Q + 2NL$
p-FHT-FSCL (sequential)	$N(L+1)Q + 2NL$

summarized in Table III.

IV. SIMULATION RESULTS

In this section, we numerically analyze the error-correction performance in terms of FER, the computational complexity, and the memory requirements of the proposed decoders and compare them with those of FSCL and RPA decoders for RM codes. We consider RM codes with $m \in \{7, 8, 9\}$ and $r \in \{2, 3, 4\}$.

A. Permuted FHT-FSC Decoding versus FSCL Decoding

Fig. 6 illustrates the error-correction performance of the conventional FSC [15] and FSCL [16] decoders, and that of the proposed permuted FHT-FSC decoder. The FSCL decoders have a list size $L \in \{2, 4, 8, 16, 32\}$ and are denoted as FSCL- L , and p-FHT-FSC- L denotes the permuted FHT-FSC decoder that uses L random permutations. In addition, the computational complexities and memory requirements of all the decoders considered in Fig. 6 are provided in Fig. 7 and Table IV, respectively.

It can be observed from Fig. 6 that in general the p-FHT-FSC- L decoder obtains significant error-correction performance gains over the FSCL- L decoders except for $\mathcal{RM}(4, 7)$. Furthermore, the p-FHT-FSC- L decoders completely remove

the need to perform path forking, path killing, and sorting operations since the decoding on each permutation is independent of the others. Therefore, the computational complexity of the p-FHT-FSC- L decoders is lower than that of the FSCL- L decoders when the list size increases, as observed in Fig. 7 for $r \in \{3, 4\}$. In particular, for the RM codes of length 128, the FER performance of the FSCL-32 decoder can be obtained by the p-FHT-FSC-32 decoder. This reduces up to 71% of the computational complexity of the FSCL-32 decoder while using a similar memory requirement as shown in Fig. 7 and Table IV, respectively. For all the RM codes of lengths 256 and 512, except for $\mathcal{RM}(4, 8)$, the error probability of the p-FHT-FSC-8 decoder is similar to or significantly better than that of FSCL-32, while only requiring up to 40% of the computational complexity and 27% of the memory requirement of the FSCL-32 decoder.

B. Permuted FHT-FSC-based Decoding versus RPA Decoding

Fig. 8 compares the error-correction performance of the permuted FHT-FSC and FHT-FSCL decoders with the state-of-the-art RPA decoding algorithm. The lower-bound of the FER values under ML decoding are also provided for comparison [11]. We consider the permuted decoders p-FHT-FSC- M and p-FHT-FSCL- L - M_L ($L \in \{2, 4\}$) where M and M_L are the number of random permutations applied to the FHT-FSC and FHT-FSCL- L decoders, respectively. We set $LM_L = M$ to maintain the same number of FSC decoding attempts under all the proposed decoders. The value of M is selected as the smallest number that enables the p-FHT-FSCL-4- M_4 decoder to have a comparable error-correction performance with that of RPA decoding at the target FER of 10^{-4} . Fig. 9 and Table V summarize the computational complexity and memory requirement of the decoders in Fig. 8.

As observed from Fig. 8, for RM codes of length 128, the error-probability of the RPA decoder can be achieved by the p-FHT-FSC- M and p-FHT-FSCL- L - M_L decoders, where the values of M are 16, 32, and 16 for $r \in \{2, 3, 4\}$, respectively. For all other RM codes considered in Fig. 8 except for $\mathcal{RM}(3, 9)$, the p-FHT-FSCL-4- M_4 decoder can provide a similar or better FER performance when compared to that of the RPA decoder at the target FER of 10^{-4} . The p-FHT-FSC- M and p-FHT-FSCL-2- M_2 decoders only incur a maximum FER degradation of 0.75 and 0.4 dB compared with the RPA decoder at the same target FER. In addition, as observed from Fig. 9, the p-FHT-FSCL-4- M_4 decoder requires a complexity that is several order-of-magnitudes lower when compared with that of the RPA decoder, while relatively achieving the FER performance of the state-of-the-art RPA decoding algorithm.

TABLE IV: Memory requirements in KB of various FSC-based and FSCL-based decoders considered in Fig. 6.

m	7						8						9					
L	1	2	4	8	16	32	1	2	4	8	16	32	1	2	4	8	16	32
FSCL- L																		
FHT-FSCL- L	1.01	1.56	2.62	4.75	9.00	17.50	2.02	3.12	5.25	9.50	18.00	35.00	4.05	6.25	10.50	19.00	36.00	70.00
p-FHT-FSC- L (parallel)																		

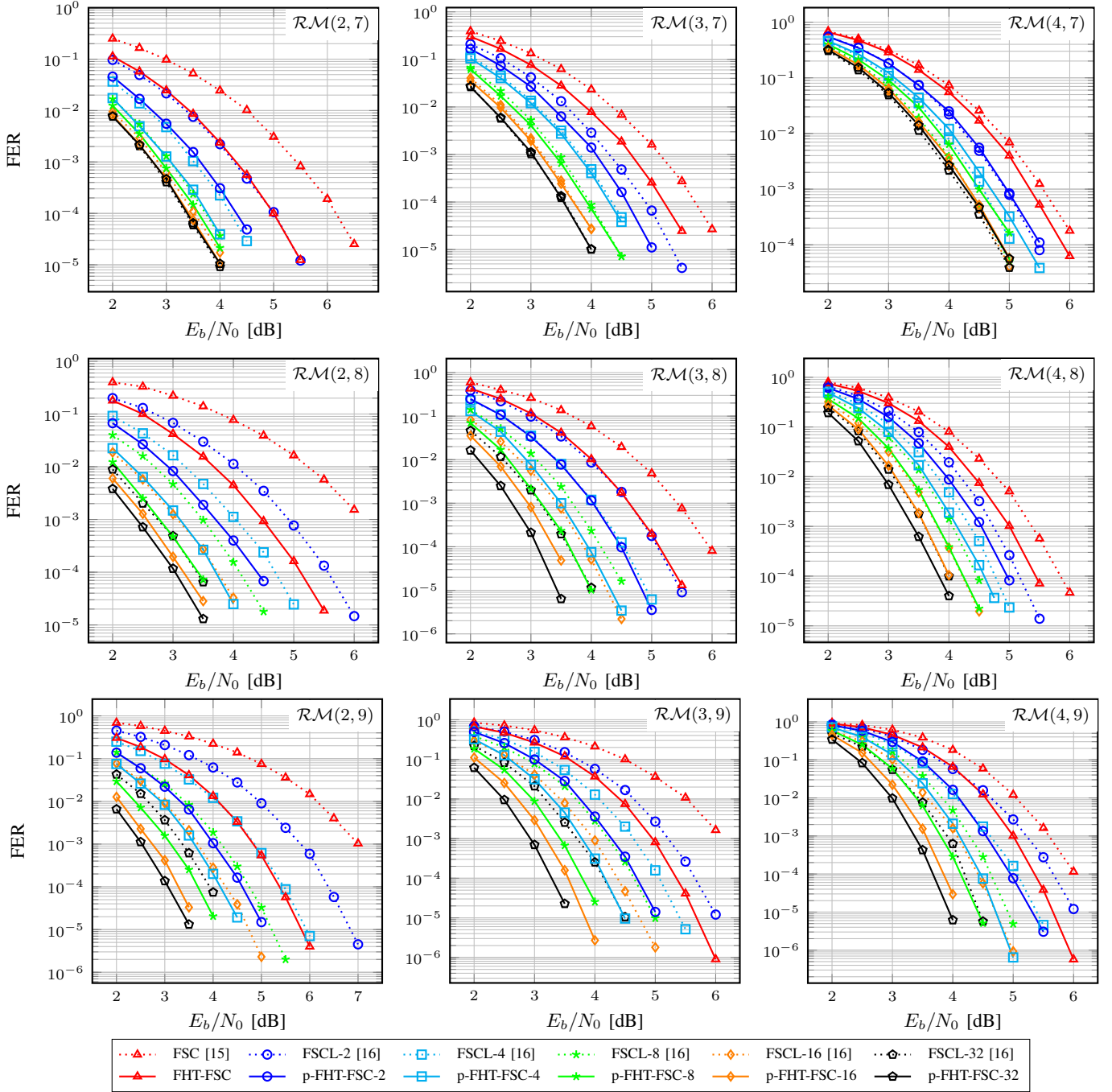


Fig. 6: Error correction performance of the FSCL and permuted FHT-FSC decoders.

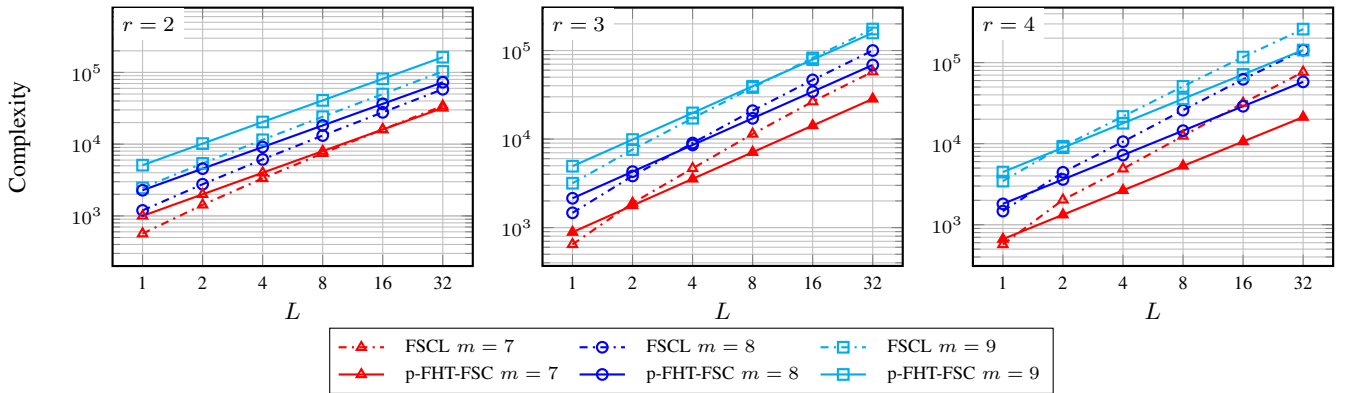


Fig. 7: Computational complexities of the FSCL and permuted FHT-FSC decoders considered in Fig. 6.

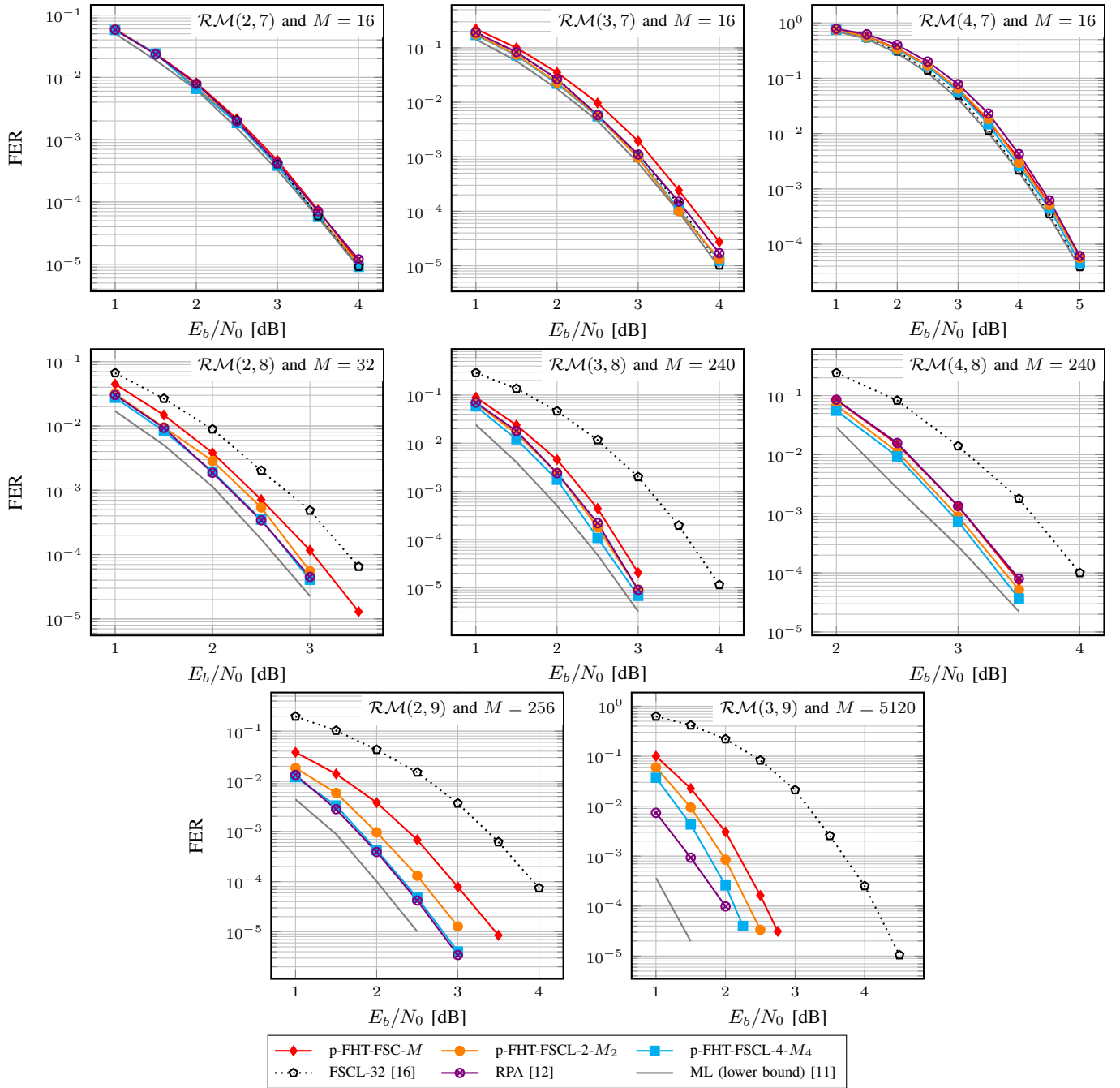


Fig. 8: Error correction performance of the RPA and the proposed decoders.

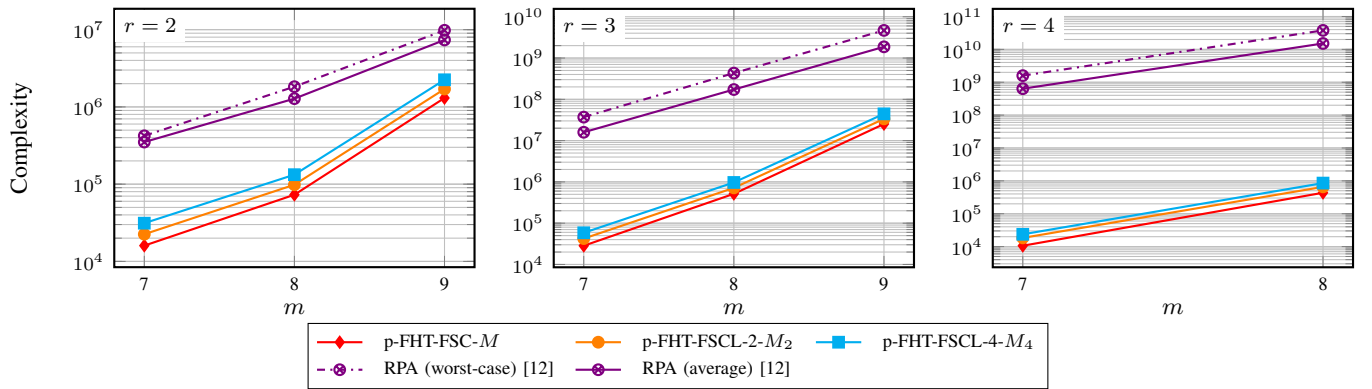


Fig. 9: Computational complexities of the RPA and the proposed decoders considered in Fig. 8.

TABLE V: Memory requirements in KB of the RPA and the proposed decoders under a sequential implementation.

Decoder	m		
	7	8	9
RPA	2.01	4.03	8.06
p-FHT-FSC- M	1.01	2.02	4.05
p-FHT-FSCL-2- M_2	1.56	3.12	6.25
p-FHT-FSCL-4- M_4	2.62	5.25	10.50

However, the p-FHT-FSCL-4- M_4 decoder incurs a maximum memory overhead of 30% compared to the RPA decoder when $m = 9$. It is worth to note that the memory consumed by the p-FHT-FSCL-4- M_4 decoder is similar to that of the conventional FSCL-4 decoder, which is a practical selection of the list size under various hardware implementations of FSCL decoding [16], [26].

V. CONCLUSION

In this paper, we proposed two decoding techniques that significantly improve the error-correction performance of FSC and FSCL decoding algorithms for short RM codes. We first integrated FHT into FSC and FSCL decoding to optimally decode the first-order RM subcodes, forming the FHT-FSC and FHT-FSCL decoding algorithms. We then ran the FHT-FSC and FHT-FSCL decoders on a list of random bit-index permutations of the codes to further improve the FER performance of FHT-FSC and FHT-FSCL decoding. We showed that for various RM codes, the permuted FHT-FSC decoder which runs on L permuted codewords outperform the FSCL decoder with list size L , while maintaining the same memory requirement and significantly reducing the computational complexity of the conventional FSCL decoder. We also showed that the permuted FHT-FSCL decoder with list size 4 can achieve a comparable error probability of state-of-the-art RPA decoding for various RM code configurations, and only requires a complexity that is several orders of magnitude lower than that of RPA decoding.

REFERENCES

- [1] D. E. Muller, "Application of boolean algebra to switching circuit design and to error detection," *Transactions of the I.R.E. Professional Group on Electronic Computers*, vol. EC-3, no. 3, pp. 6–12, 1954.
- [2] I. Reed, "A class of multiple-error-correcting codes and the decoding scheme," *Transactions of the IRE Professional Group on Information Theory*, vol. 4, no. 4, pp. 38–49, 1954.
- [3] E. Arıkan, "Channel polarization: A method for constructing capacity-achieving codes for symmetric binary-input memoryless channels," *IEEE Trans. Inf. Theory*, vol. 55, no. 7, pp. 3051–3073, July 2009.
- [4] I. Tal and A. Vardy, "How to construct polar codes," *IEEE Trans. Inf. Theory*, vol. 59, no. 10, pp. 6562–6582, 2013.
- [5] P. Trifonov, "Efficient design and decoding of polar codes," *IEEE Trans. Commun.*, vol. 60, no. 11, pp. 3221–3227, 2012.
- [6] L. Huang, H. Zhang, R. Li, Y. Ge, and J. Wang, "Reinforcement learning for nested polar code construction," *IEEE Global Commun. Conf.*, pp. 1–6, 2019.
- [7] Y. Liao, S. A. Hashemi, J. Cioffi, and A. Goldsmith, "Construction of polar codes with reinforcement learning," *IEEE Global Commun. Conf. (to appear)*, 2020. [Online]. Available: <https://arxiv.org/abs/2009.09277>
- [8] I. S. Reed, "A class of multiple-error-correcting codes and the decoding scheme," Massachusetts Inst of Tech Lexington Lincoln Lab, Tech. Rep., 1953.

- [9] V. M. Sidel'nikov and A. Pershakov, "Decoding of reed-muller codes with a large number of errors," *Problemy peredachi informatsii*, vol. 28, no. 3, pp. 80–94, 1992.
- [10] B. Sakkour, "Decoding of second order reed-muller codes with a large number of errors," in *IEEE Information Theory Workshop, 2005.*, 2005.
- [11] I. Dumer and K. Shabunov, "Soft-decision decoding of reed-muller codes: recursive lists," *IEEE Trans. Inf. Theory*, vol. 52, no. 3, pp. 1260–1266, 2006.
- [12] M. Ye and E. Abbe, "Recursive projection-aggregation decoding of reed-muller codes," *IEEE Trans. Inf. Theory*, vol. 66, no. 8, pp. 4948–4965, 2020.
- [13] Y. Be'ery and J. Snyders, "Optimal soft decision block decoders based on fast hadamard transform," *IEEE Trans. Inf. Theory*, vol. 32, no. 3, pp. 355–364, 1986.
- [14] M. Hashemipour-Nazari, K. Goossens, and A. Balatsoukas-Stimming, "Hardware implementation of iterative projection-aggregation decoding of reed-muller codes," 2020. [Online]. Available: <https://arxiv.org/abs/2012.00581>
- [15] G. Sarkis, P. Giard, A. Vardy, C. Thibault, and W. J. Gross, "Fast polar decoders: Algorithm and implementation," *IEEE J. Sel. Areas Commun.*, vol. 32, no. 5, pp. 946–957, April 2014.
- [16] S. A. Hashemi, C. Condo, and W. J. Gross, "Fast and flexible successive-cancellation list decoders for polar codes," *IEEE Trans. on Sig. Proc.*, vol. 65, no. 21, pp. 5756–5769, Nov 2017.
- [17] D. Fathollahi, N. Farsad, S. A. Hashemi, and M. Mondelli, "Sparse multi-decoder recursive projection aggregation for reed-muller codes," 2020. [Online]. Available: <https://arxiv.org/abs/2011.12882>
- [18] N. Hussami, S. B. Korada, and R. Urbanke, "Performance of polar codes for channel and source coding," in *IEEE Int. Symp. on Inf. Theory*, 2009, pp. 1488–1492.
- [19] A. Elkelesh, M. Ebada, S. Cammerer, and S. ten Brink, "Belief propagation list decoding of polar codes," *IEEE Commun. Letters*, vol. 22, no. 8, pp. 1536–1539, 2018.
- [20] M. Geiselhart, A. Elkelesh, M. Ebada, S. Cammerer, and S. ten Brink, "Automorphism ensemble decoding of reed-muller codes," 2020. [Online]. Available: <https://arxiv.org/abs/2012.07635>
- [21] N. Doan, S. A. Hashemi, M. Mondelli, and W. J. Gross, "On the decoding of polar codes on permuted factor graphs," *IEEE Global Commun. Conf.*, pp. 1–6, Dec 2018.
- [22] S. A. Hashemi, N. Doan, M. Mondelli, and W. J. Gross, "Decoding reed-muller and polar codes by successive factor graph permutations," in *2018 IEEE 10th International Symposium on Turbo Codes Iterative Information Processing (ISTC)*, 2018, pp. 1–5.
- [23] E. Arıkan, "A survey of reed-muller codes from polar coding perspective," in *IEEE Inf. Theory Work. on Inf. Theory*, 2010, pp. 1–5.
- [24] —, "A performance comparison of polar codes and reed-muller codes," *IEEE Commun. Lett.*, vol. 12, no. 6, pp. 447–449, 2008.
- [25] I. Tal and A. Vardy, "List decoding of polar codes," *IEEE Trans. Inf. Theory*, vol. 61, no. 5, pp. 2213–2226, March 2015.
- [26] A. Balatsoukas-Stimming, M. B. Parizi, and A. Burg, "LLR-based successive cancellation list decoding of polar codes," *IEEE Trans. Signal Process.*, vol. 63, no. 19, pp. 5165–5179, Oct. 2015.
- [27] A. Alamdar-Yazdi and F. R. Kschischang, "A simplified successive-cancellation decoder for polar codes," *IEEE Commun. Lett.*, vol. 15, no. 12, pp. 1378–1380, October 2011.
- [28] M. H. Ardakani, M. Hanif, M. Ardakani, and C. Tellambura, "Fast successive-cancellation-based decoders of polar codes," *IEEE Trans. Commun.*, vol. 67, no. 7, pp. 4562–4574, 2019.
- [29] S. A. Hashemi, C. Condo, F. Ercan, and W. J. Gross, "Memory-efficient polar decoders," *IEEE J. Emerg. Sel. Topics Circuits Syst.*, vol. 7, no. 4, pp. 604–615, Dec. 2017.
- [30] N. Doan, S. A. Hashemi, and W. J. Gross, "Decoding polar codes with reinforcement learning," *IEEE Global Commun. Conf. (to appear)*, 2020. [Online]. Available: <https://arxiv.org/abs/2009.06796>